The microstructural influence of nitrogen incorporation in dilute nitride semiconductors

2004 J. Phys.: Condens. Matter 16 S3161

(http://iopscience.iop.org/0953-8984/16/31/012)

INSTITUTE OF PHYSICS PUBLISHING JOURNAL OF PHYSICS: CONDENSED MATTER

J. Phys.: Condens. Matter **16** (2004) S3161–S3170 PII: S0953-8984(04)75283-2

The microstructural influence of nitrogen incorporation in dilute nitride semiconductors

P R Chalker, T J Bullough, M Gass, S Thomas and T B Joyce

Materials Science and Engineering, The University of Liverpool, Liverpool L69 3GH, UK

Received 19 January 2004
Published 23 July 2004
Online at stacks.iop.org/JPhysCM/16/S3161
doi:10.1088/0953-8984/16/31/012

Abstract

The influence of nitrogen incorporation on the microstructure of dilute nitride films and quantum wells has been investigated using cross-section scanning transmission electron microscopy. The elemental distributions of Ga, In, N and As in GaInNAs and GaAsN films have been mapped by energy dispersive x-ray analysis. Below the solubility limit for nitrogen, homogeneous GaAsN and GaInNAs compositions are obtained of good crystalline quality near to the epilayer/GaAs interface. In GaAsN films containing nitrogen above the solubility limit a graded transition from arsenide-like to nitride-like material occurs after some 50 nm of growth. GaInNAs films containing nitrogen exceeding the solubility limit exhibit a 'cellular' microstructure consisting of a gallium-depleted InGaAs centre with walls of a GaN-like composition. A similar segregation effect is observed in GaInNAs quantum wells containing nitrogen around and above the solubility limit. The formation of In-rich regions occurs within the wells, which causes three-dimensional growth at higher nitrogen contents, with the consequent initiation of growth defects. The electronic structure of GaInNAs quantum wells has been investigated by mapping the variation in the plasmon frequency using electron energy loss spectrometry on a dedicated scanning transmission electron microscope. Kramers–Kronig analysis of the singly scattered low-loss region yields a measure of the local effective valence electron density.

(Some figures in this article are in colour only in the electronic version)

1. Introduction

The on-going development of dilute nitrides such as GaNAs and GaInNAs is the focus of a considerable research activity because of their potential application across a range of device applications including lasers [1–6], photodetectors [7], solar cells [8] and transistors [9]. The term dilute nitride is widely used to describe III–V semiconductors consisting of a low nitrogen (<5%) content. Although the fraction of the group V element which is substituted for by nitrogen is relatively low, the smaller ionic radius of the nitrogen is observed to dramatically

decrease the bandgap energy and decrease the lattice parameter. It was proposed by Kondow *et al* [10] that increasing the indium fraction in the quaternary GaInNAs alloy reduces the bandgap but also increases the lattice parameter. This makes it possible to balance the nitrogen and indium contents of GaInNAs to target a narrow-bandgap material and near lattice parameter matching to substrate materials such as gallium arsenide.

The large lattice parameter difference between GaAs and cubic GaN (20%) makes the ternary GaAsN alloy scientifically interesting. Since GaAsN is generally grown on GaAs substrates, strain arising from the mismatch will have an enormous effect on any alloy epilayer properties. Neugebauer and Van de Walle [11] have estimated that the equilibrium solubility of nitrogen in GaAs is of the order of only 2 at.%, making it necessary to use non-equilibrium growth methods. Due to its large miscibility gap GaAsN tends to phase separate when the nitrogen content becomes appreciable [12]; however, nitrogen incorporation up to nearly 15% has been reported using a nitrogen plasma source combined with a relatively low growth temperature of 500 °C on a GaP substrate [13].

The large body of data available for the quaternary GaInNAs alloy regarding the luminescence from low-nitrogen-containing (<1%) quantum-well-based structures indicates their emission wavelength falls just below 1.3 μm at room temperature for indium contents below 30% [14]. It has also been noted that the addition of higher nitrogen concentrations rapidly degrades the microstructure, preventing its use in optical devices. Some reports of higher-nitrogen-containing materials have been made and, in particular, GaInNAs quantum dots with 4% nitrogen have been observed to give peak emission characteristics up to 1.5 μm [15].

In this paper we have investigated the microstructure of dilute-nitride films and quantum wells using transmission electron microscopy (TEM) to compare the influence of nitrogen additions above and below the solubility limit; and to investigate the influence of adding indium to these materials.

2. Experimental procedure

A VG V80H chemical beam epitaxy (CBE) system configured for all vapour sources was used to grow all material samples. Triethylgallium (TEG) and trimethylindium (TMIn) were used as the group III precursors and arsine (AsH_3) was pre-cracked to give an As_2 flux. An Oxford Applied HD25 RF atom source was used to inject an atomic nitrogen plasma flux into the chamber, with flow rates between 1 and 5 sccm and forward power $\sim$ 100 W. Substrates were epi-ready (001) GaAs that were cleaned under an arsenic flux so that all surface oxides were desorbed. For the deposition of GaAsN and GaInNAs films, a 200 nm GaAs buffer layer was grown at 550 °C and then $\sim$300 nm GaAsN or GaInNAs layers were deposited at $\sim$500 °C using a growth rate of 1 μm h^{-1}. The fluxes were adjusted to give a N incorporation of about 4% of group V elements (just below the solubility limit) and 10% (well above the solubility limit), with an In fraction of 0.22 in the GaInAsN determined by secondary ion mass spectrometry. The level of nitrogen incorporation was estimated from the frequency of the LO_2 phonon measured by Raman spectroscopy [16].

For the GaInNAs quantum well and laser structures, GaAs(001) epi-ready substrates were thermally cleaned under an As_2 flux and a 200 nm GaAs buffer layer was grown at 550 °C. 7 nm $Ga_xIn_{1-x}As_{1-y}N_y$ wells were grown at either the same temperature or 490 °C. Details of the particular well compositions are described below. The indium and nitrogen concentrations in the quantum well were established using dynamic secondary ion mass spectrometry and photoluminescence measurements with a calibration sample [17].

Ion-beam-thinned cross-section samples were examined using a VG microscope HB601 UX field emission gun scanning transmission electron microscope (STEM) operating at 100 kV,

giving a 1 nm focused electron probe at the specimen, and a JEOL 2000FX TEM operating at 200 kV. Samples were aligned with either [110] or [$\bar{1}$10] parallel to the electron transmission axis. Acquisition of energy dispersive x-ray (EDX) spectra, line scans and maps was performed on the STEM using a LINK eXL system with a LINK windowless x-ray detector. The STEM is also equipped with a Gatan Enfina electron energy loss spectrometer and is capable of producing a 0.35 eV FWHM zero-loss peak. The system is able to acquire images and 3D data cubes containing an electron energy loss spectrum at each pixel in the map, enabling imaging of energy loss features such as the bulk plasmon frequency.

3. Results and discussion

3.1. GaAsN and GaInNAs films

Bright-field TEM cross-sections and EDX elemental maps of GaNAs films grown with nitrogen levels (a) below and (b) above the solubility limit are compared in figure 1. The low-nitrogen-containing film is characterized by elemental maps showing relatively uniform elemental distributions, representative of an essentially homogeneous composition. The nitrogen content of this GaAsN specimen is below the detection limit of the EDX. Some of the crystalline defects present in the layer, such as twins and threading dislocations, originate at the GaAs/GaAsN interface, although a few have their origin within the GaAs buffer layer. By contrast, the high-nitrogen-content film shown in figure 1(b) exhibits a relatively featureless initial 50 nm of growth, after which the microstructure degrades. The EDX maps of this high-N-content layer show a relatively uniform elemental composition across the interface between the GaAs buffer and GaAsN layer. However, the EDX maps clearly show a decrease of As and increase of N intensity associated with the degradation of the GaAsN epilayer. About 50 nm from the buffer layer the GaAsN structure degrades and the As and N concentrations become constant. EDX line scans indicate that the near-surface As concentration is less than 25% of that at the start of the GaAsN layer. This observation suggests that the incorporation ratio of N:As increases during the growth of the GaAsN layer despite the constant nitrogen and arsenic fluxes used during growth.

Figure 2(a) shows a bright-field cross-section image and EDX elemental maps of a GaInNAs film with a low nitrogen (4% of group V elements) fraction. Although the various elemental concentrations remain relatively constant throughout the layer, after about 50 nm of good epitaxial growth the GaInAsN layer becomes increasingly defective and rough.

Figure 2(b) shows the comparable high-nitrogen-content (10% of group V elements) GaInNAs layer. The microstructure projected through the thickness of the sample cross-section consists of 'platelets' or 'cells'. These are of the order of 30–50 nm in size perpendicular to the growth surface, and ∼80 nm in width parallel to the surface along the [110] direction, although the structure of these cellular features is anisotropic [18]. Each platelet is separated from one another by a 5–10 nm layer of a second phase. The intensity of the elemental maps from this sample clearly shows the presence of In, Ga and As within the platelets. The indium composition appears to vary across each platelet, becoming In rich towards the centre. A high concentration of twins and other defects is seen in many of the platelets. The thin second-phase layer separating the platelets consists of a material with increased gallium content and a deficiency in In and As. Although no clear indication of nitrogen can be associated with this second phase from the maps shown in figure 2(b), EDX line scans and maps from other samples show a direct correlation, indicating this layer is gallium nitride-like in composition.

The growth mechanisms taking place at the surface during CBE deposition are more complex than in MBE, involving molecular decomposition of the metal–organics as well as surface diffusion. Compositional variations in III–V thin films, including InGaAs and

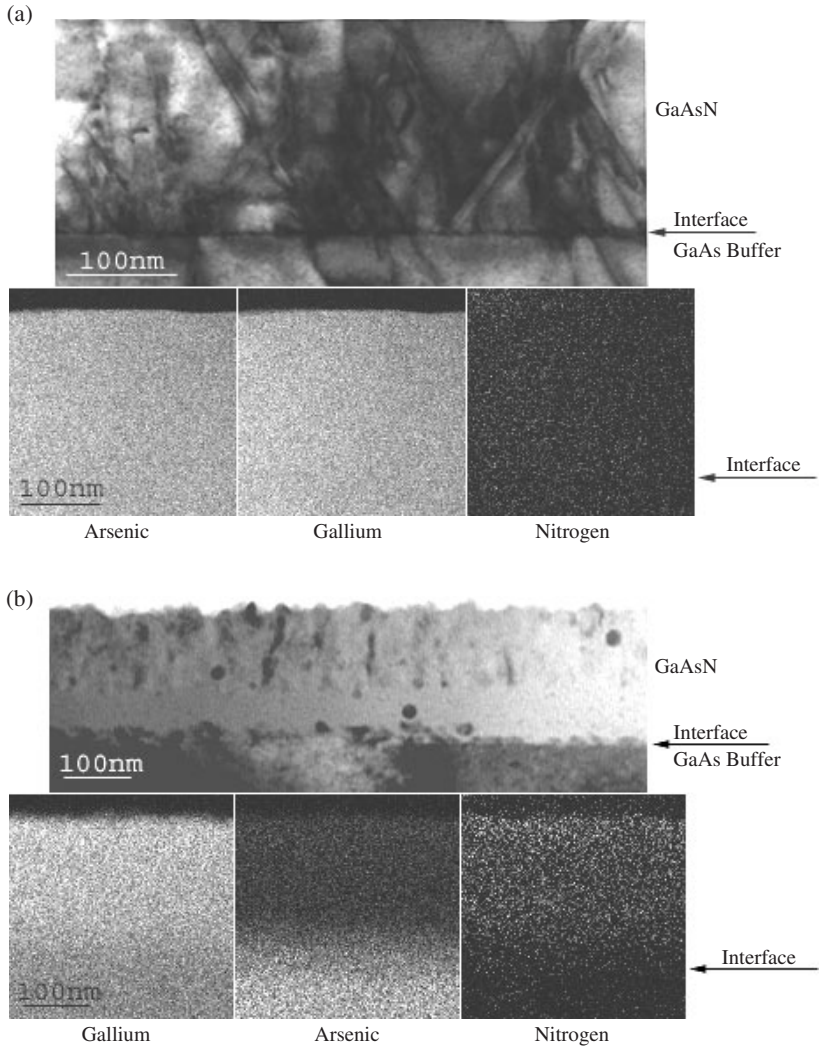

Figure 1. Bright-field transmission electron micrographs and energy dispersive x-ray maps of the Ga, As and N elemental distributions from cross-sections of GaAsN containing (a) 4% nitrogen and (b) 10% nitrogen.

InGaN, have been previously reported and have been attributed to strain [19], or a difference in adsorbate mobility [20–23]. The observations presented here of phase-separated GaInNAs growth are very similar to the 'natural' superlattices observed in InAsSb films below a critical growth temperature [24], and are consistent with the phase separation taking place at the surface during growth, with nearly complete phase separation (into InGaAs or GaInNAs, and GaN) resulting from islands of the two different phases forming on the surface which then laterally overgrow each other.

3.2. The influence on nitrogen on GaInNAs QW microstructure

The distribution of indium and nitrogen in GaInNAs QWs has a significant effect on their emission characteristics [25]. Previously, transmission electron microscopy has been

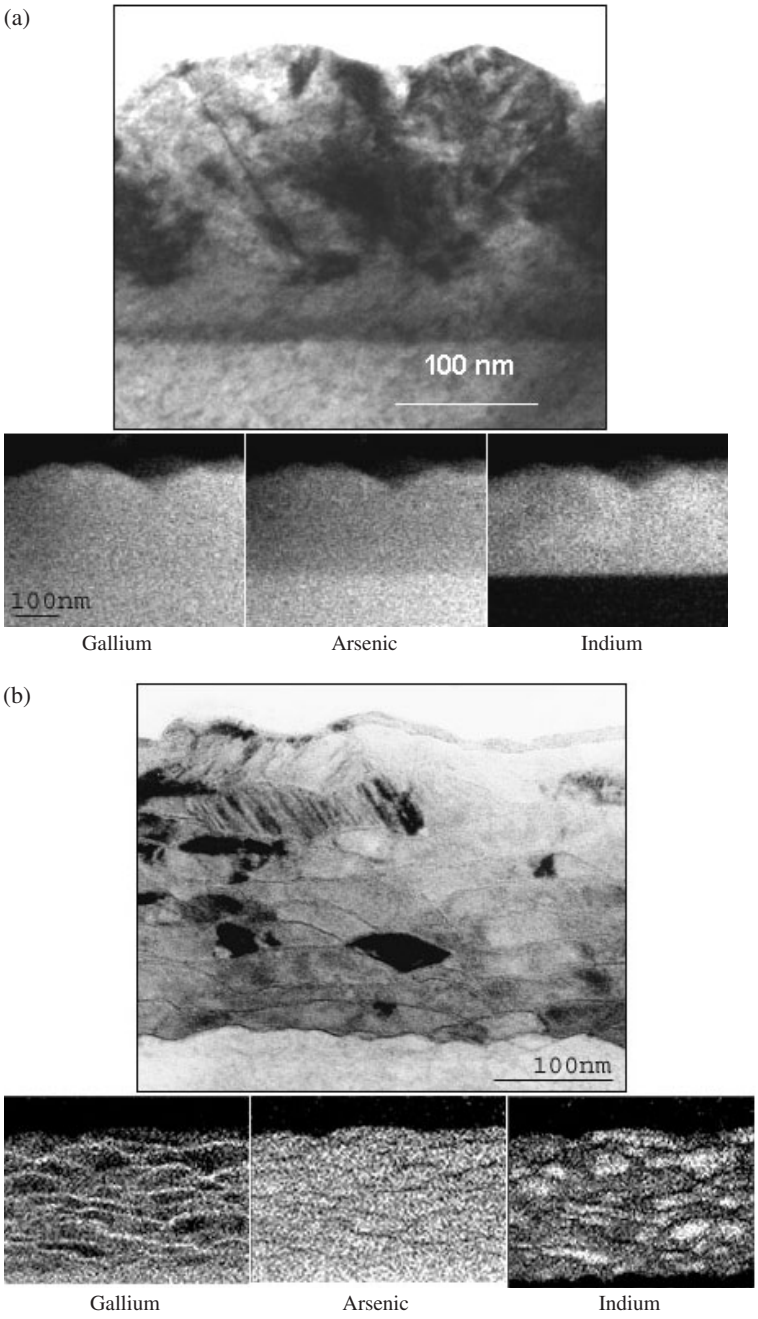

Figure 2. Bright-field transmission electron micrographs and energy dispersive x-ray maps of the Ga, As and In elemental distributions from GaInAsN cross-sections with (a) 4% nitrogen content and (b) 10% nitrogen content.

used to reveal the formation of quantum-dot-like features in GaInNAs quantum wells via atomic number contrast [26]. The dot structures were explained in terms of non-uniform N and In compositions with the quantum well. A comparison of $Ga_{0.7}In_{0.3}As/GaAs$ and

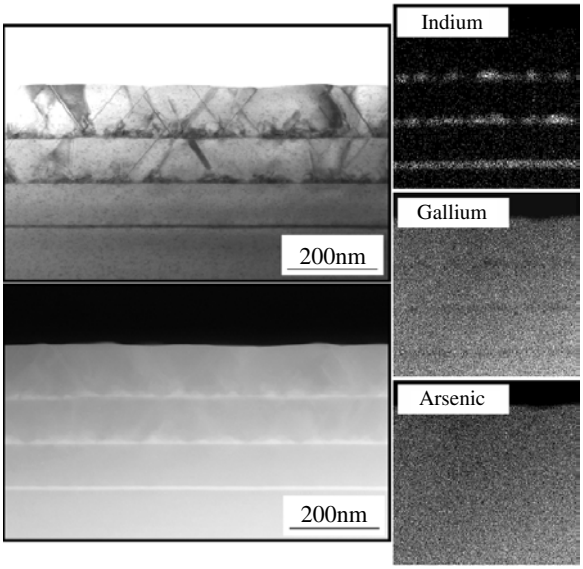

Figure 3. STEM BF, DF and EDX micrographs indicating the degradation of the quantum wells grown with increasing nitrogen concentration.

$Ga_{0.7}In_{0.3}N_{0.02}As_{0.98}$/GaAs wells showed a similar undulating structure that was attributed to lateral variations in strain. The effect was more pronounced in the nitrogen-containing quantum wells, which was attributed to non-uniform In and N concentrations.

More recently [27], the variation of elemental composition in as-grown GaInNAs/GaAs quantum well structures has been investigated by energy dispersive x-ray analysis of cross-sections using a dedicated FEG STEM. The formation of quaternary GaInNAs dot structures was indicated by low-temperature photoluminescence measurements and by the correlation of indium and nitrogen distributions. The distributions of arsenic and nitrogen across the well structure suggested the presence of a continuous nitride-like layer formed at the surface of the GaAs buffer layer, which was responsible for the GaInNAs dot formation.

To explore the influence of nitrogen content on the microstructure of GaInNAs quantum wells further, a sample was grown consisting of a triple-quantum-well structure comprising wells with increasing levels of nitrogen of about 2%, 4% and 6% of the group V elements respectively. Figure 3 shows a bright-field image of a cross-section of this sample. The first quantum well deposited exhibits a homogeneous contrast with a high degree of elemental uniformity within the 8 nm well. The well is flat and defect free across the whole region investigated. The first GaAs spacer layer has a thickness of ∼90 nm and consists of an epitaxial layer forming a good surface for the second quantum well. In contrast to the first QW the second GaInNAs layer exhibits a high level of segregation within the well into 'islands' containing enhanced levels of indium. The second well contains approximately double the nitrogen content of the first, and it is apparent that homogeneous deposition is replaced by the initiation of a segregated structure. The consequent roughening of the growth surface degrades the crystal quality as dislocations are initiated, hindering any further planar overgrowth. This morphological degradation becomes more dramatic in the third well where almost total segregation of the GaInNAs material has occurred, resulting in very distinct regions which are both In and N rich. The crystal defect density also increases with progressively higher nitrogen content, resulting in a progressively rougher growth surface.

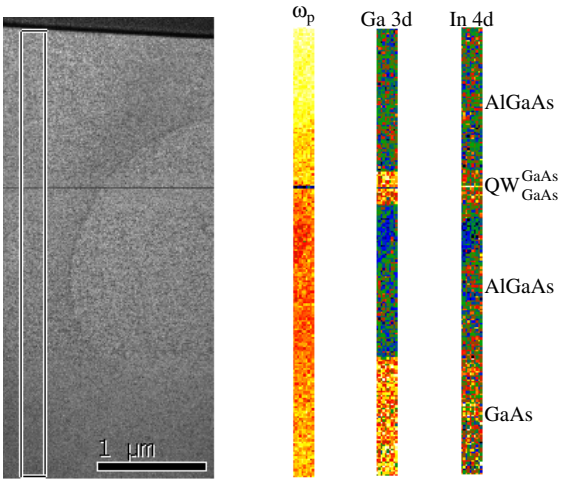

Figure 4. Bright-field image of a cross-section through a GaInNAs/GaAs quantum well laser structure. The boxed region highlights the area where a map of the plasmon frequency shift ω_p is recorded and maps of the Ga 3d and In 4d EELS transition have been produced. The plasmon frequency ranges from 2.401×10^{16} to 2.438×10^{16} s^{-1}; the Ga 3d and In 4d transitions are arbitrary units.

The incorporation of indium and nitrogen in GaInNAs are related in a complex manner [28, 29] depending on growth temperature and rate. Also, the strain induced in the structures originating from the GaInNAs wells may favour the formation of self-assembled island structures [30, 31], possibly leading to a type of 'quantum dot' formation. The result of non-uniform elemental distribution is localized strain variations within the wells, and at the interfaces between the wells and the surrounding GaAs matrix [32].

3.3. Imaging of the electronic structure of GaInNAs QWs

In addition to the physical distribution of elements within a material, scanning transmission electron microscopy is capable of imaging the local electronic structure via electron energy loss processes of the primary electron probe. The energy loss spectrum (ELS) of these features includes a characteristic plasmon peak, which is observed in each spectrum in addition to characteristic elemental edges. The observed plasmon frequency ω_p is given by

$$\omega_p = \left(\frac{ne^2}{m_e^* \varepsilon_0}\right)^{1/2} \tag{1}$$

where n is the electron density, e the electronic charge, ε_0 the permittivity of free space and m_e^* the electron effective mass. The plasmon energy can be used to form a map that is sensitive to (i) the local chemistry of the specimen through n_{eff} that reflects the density of valence electrons of atoms present and (ii) the local band structure reflected by variations in the electron effective mass [33]. This is illustrated in figure 4, which shows a bright-field image of a cross-section through a GaInNAs/GaAs laser structure incorporating a 7 nm GaInNAs quantum well clad by gallium arsenide. Above and below the GaAs layers are p- and n-type AlGaAs confinement layers. The inset shows an area from which ELS data was collected. A false colour map of ω_p, the variation in frequency of the plasmon peak intensity, is shown for this area. The variation in plasmon frequency reflecting the local variation in n_{eff} and m_e^* due to the different arsenide phases is clearly visible. The GaInNAs quantum well can also be clearly distinguished.

The Ga 3d and In 4d false colour maps are taken from the imaginary part of the dielectric function, ε_2, obtained through Kramers–Kronig analysis described below, at energy slices of 20.0–24.0 and 18.5–19.6 eV respectively, and represent the transitions from the Ga 3d and In 4d levels to the conduction band. As these transitions closely follow the plasmon peak in energy, it is difficult to fit an accurate background; however, in ε_2 the plasmon peak is not observed, so it is somewhat easier to find an appropriate background fit. It has also been shown that whilst changes in sample thickness can affect the quantification in single-scattered distribution (SSD), the transitions in ε_2 are not affected [34]. The change in percentage Ga is clearly seen in the Ga 3d map, with a noticeable reduction of intensity in the AlGaAs layers, and even greater within the QW. The In 4d map, however, only shows an increase in intensity within the QW, as expected.

The energy loss spectrum associated with each pixel is closely related to the energy loss function, $\mathrm{Im}[-1/\varepsilon(E)]$, via the relationship

$$S(E) = K\,\mathrm{Im}\left[\frac{-1}{\varepsilon(E)}\right]\ln\left[1+\frac{\beta^2}{\theta_E^2}\right] \tag{2}$$

where $S(E)$ is the single-scattering distribution. K is a proportionality constant with a dependence on the specimen thickness, incident beam energy and zero-loss intensity. β and θ_E are the effective collection and characteristic scattering angles respectively. Consequently, the energy loss function can be obtained from the low-loss spectrum after the removal of the zero-loss peak and plural-scattering features. The energy loss function is related to the quantity $\mathrm{Re}[1/\varepsilon(E)]$ via the Kramers–Kronig transformation,

$$\mathrm{Re}\left[\frac{1}{\varepsilon(E)}\right] = 1 - \frac{2}{\pi}P\int_0^\infty \mathrm{Im}\left[\frac{-1}{\varepsilon(E')}\right]\frac{E\,\mathrm{d}E'^2}{E'^2-E^2} \tag{3}$$

where P indicates the Cauchy principal part of the integral. Calculation of the transform is achieved efficiently using a Fourier-based procedure [35]. The real and imaginary parts of the dielectric function $\varepsilon_1(E)$ and $\varepsilon_2(E)$ are calculated from $\mathrm{Im}[-1/\varepsilon(E)]$ and $\mathrm{Re}[1/\varepsilon(E)]$ using the relationship

$$\varepsilon(E) = \varepsilon_1(E) + \mathrm{i}\varepsilon_2(E) = \frac{\mathrm{Re}\big[1/\varepsilon(E)\big] + \mathrm{i}\,\mathrm{Im}\big[-1/\varepsilon(E)\big]}{\big\{\mathrm{Re}\big[1/\varepsilon(E)\big]\big\}^2 + \big\{\mathrm{Im}\big[-1/\varepsilon(E)\big]\big\}^2}. \tag{4}$$

The imaginary part $\varepsilon_2(E)$ of the dielectric function can be used to compute the effective number of electrons per unit volume n_eff, using equation (5) where $\hbar$ is the Planck constant.

$$n_\mathrm{eff}(\varepsilon_2) = \frac{2\varepsilon_0 m_0}{\pi\hbar^2 e^2}\int_0^\infty E'\varepsilon_2(E')\,\mathrm{d}E'. \tag{5}$$

The local effective electron concentration, n_eff, can be calculated from equation (5) and substituted into equation (1) to provide an estimate of the local electron effective mass (m_e^*) [36]. Figure 5 shows a map of the variation of m_e^* in a GaInNAs/GaAs QW which ranges from 0.0814 m_e^* (blue/black) to 0.0862 m_e^* (yellow/white) within the quantum well. Increasing the indium content in GaInAs decreases m_e^*. However, comparison of the m_e^* and In 4d maps indicates an increase in m_e^* coupled with the local indium concentration. The electron effective mass of a GaInAs alloy of comparable composition would be predicted to be $0.0629\,m_0$ according to the relationship $m_\mathrm{e}^*(\mathrm{Ga}_x\mathrm{In}_{1-x}\mathrm{As}) = 0.026 + (0.041x)$ [37]. A number of groups have investigated the influence of composition in dilute nitrides upon m_e^*. These studies generally indicate that the incorporation of nitrogen into GaInAs increases m_e^* [37–45], which supports the present observations. Further investigation is required to correlate m_e^* with the local nitrogen content which is hampered by the sensitivity of these techniques to lowlevels

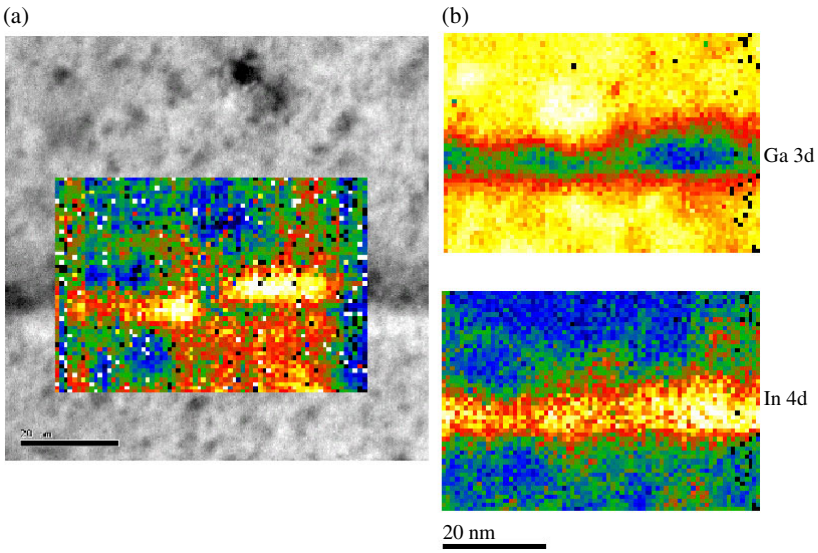

Figure 5. (a) Bright-field image of 7 nm GaInNAs/GaAs quantum well. Inset is a map of the effective mass m^* within the quantum well ranging from 0.0814 to 0.0862 m_e. (b) Maps of the Ga and In distributions obtained from the intensity of the Ga 3d and In 4d ELS transitions.

of nitrogen; however, the approach developed here enables variations in m_e^* to be mapped in GaInNAs-based semiconductor device structures.

4. Conclusions

The influence of nitrogen incorporation on the microstructure of GaAsN and GaInNAs shows marked changes above and below the solubility limit of nitrogen. GaAsN and GaInNAs specimens containing nitrogen below the solubility limit exhibit homogeneous compositions. These layers show strong crystalline contrast and have high concentrations of defects such as threading dislocations and twin boundaries. Above the nitrogen solubility limit GaAsN specimens develop a microstructure during growth consisting of a graded transition from arsenic rich at the GaAs substrate interface to nitrogen rich at the free growth surface. Raman spectroscopy shows characteristic GaN-like and GaAs-like modes, indicating the GaAsN is spinodally decomposed. GaInNAs films containing nitrogen above the solubility limit show a 'cellular' microstructure consisting of a gallium-depleted InGaAs nucleus with cell wells consisting of a GaN-like composition. This microstructure is analogous to 'natural' superlattices observed in InAsSb films below a critical growth temperature.

Mapping of the plasmon energy loss in GaInNAs quantum well structures has been used to examine local variations in chemical composition and electronic band structure. The local effective electron density can be deduced from Kramers–Kronig analysis of the energy loss spectrum for the GaInNAs well.

Acknowledgments

The authors are grateful to Professor Naci Balkan and Simone Mazzucato for the photoluminescence measurements and interpretation. We are also grateful to the Engineering and Physical Sciences Research Council for supporting this work under contracts GR/N07813.

References

[1] Larson M C, Kondow M, Kitatani T, Yazawa Y and Okai M 1997 *Electron. Lett.* **33** 959–60
[2] Larson M C, Kondow M, Kitatani T, Tamura K, Yazawa Y and Okai M 1997 *IEEE Photon. Technol. Lett.* **9** 1549–51
[3] Larson M C, Kondow M, Kitatani T, Nakahara K, Tamura K, Inoue H and Uomi K 1998 *IEEE Photon. Technol. Lett.* **10** 188–90
[4] Ellmers C, Hohnsdorf F, Koch J, Agert C, Leu S, Karaiskaj D, Hofmann M, Stolz W and Ruhle W W 1999 *Appl. Phys. Lett.* **74** 2271–3
[5] Wagner A, Ellmers C, Hohnsdorf F, Koch J, Agert C, Leu S, Hofmann M, Stolz W and Ruhle W W 2000 *Appl. Phys. Lett.* **76** 271–2
[6] Coldren C W, Larson M C, Spruytte S G and Harris J S 2000 *Electron. Lett.* **36** 951–2
[7] Heroux J B, Yang X and Wang W I 1999 *Appl. Phys. Lett.* **75** 2716–8
[8] Kurtz S R, Allerman A A, Jones E D, Gee J M, Banas J J and Hammons B E 1999 *Appl. Phys. Lett.* **74** 729–31
[9] Xin H P, Tu C W and Geva M 1999 *Appl. Phys. Lett.* **75** 1416–8
[10] Kondow M, Uomi K, Niwa A, Kitatani T, Watahiki S and Yazawa Y 1996 *Japan. J. Appl. Phys.* **35** 1273
[11] Neugebauer J and Van de Walle C G 1995 *Phys. Rev.* B **51** 10568
[12] Foxon C T *et al* 1995 *J. Cryst. Growth* **150** 892
[13] Bi W G and Tu C W 1997 *Appl. Phys. Lett.* **70** 1608
[14] Potter R J, Balkan N, Adams M J, Chalker P R, Joyce T B and Bullough T J 2000 *SPIE* (parts 1 and 2) **3944** 900–9 ISBN: 0-8194-3561-9
[15] Sopanen M, Xin H P and Tu C W 2000 *Appl. Phys. Lett.* **76** 994
[16] Thomas S, White S, Chalker P R, Bullough T J and Joyce T B 2002 *J. Mater. Sci. Mater. Electron.* **13** 525–9
[17] Mazzucato S, Potter R J, Erol A, Balkan N, Chalker P R, Thomas S, Joyce T B and Bullough T J 2003 *Solid State Electron.* **47** 483–7
[18] Thomas S, Bullough T J, Joyce T B, Zheng J-G and Chalker P R 2001 *Microscopy of Semiconducting Materials* (*Inst. Phys. Conf. Ser. 169*) p 123
[19] Tersoff J 1998 *Phys. Rev. Lett.* **81** 3183
[20] Venezuela P and Tersoff J 1998 *Phys. Rev.* B **58** 10871
[21] Cullis A G, Norris D J, Walther T, Migliorato M A and Hopkinson M 2002 *Phys. Rev.* B **66** 081305(R)
[22] Walther T, Cullis A G, Norris D J and Hopkinson M 2001 *Phys. Rev. Lett.* **86** 2381
[23] Albrecht M *et al* 2001 *Microscopy of Semiconducting Materials 2001* (*Inst. Phys. Conf. Ser. 169*) p 267
[24] Norman A G, Seong T-Y, Ferguson I T, Booker G R and Joyce B A 1993 *Semicond. Sci. Technol.* **8** S9–15
[25] Potter R J, Balkan N, Adams M J, Chalker P R, Joyce T B and Bullough T J 2000 *Proc. SPIE* **3944** 900
[26] Xin H P, Kavanagh K L, Zhu Z Q and Tu C W 1999 *Appl. Phys. Lett.* **74** 2337
[27] Chalker P R, Davock H, Thomas S, Joyce T B, Bullough T J, Potter R J and Balkan N 2001 *J. Cryst. Growth* **233** 1
[28] Miyamoto T, Kageyama T, Makino S, Schlenker D, Koyama F and Iga K 2000 *J. Cryst. Growth* **209** 339–44
[29] Friedman D, Geisz J, Kurtz S and Olson J 1998 *J. Cryst. Growth* **195** 409–15
[30] Wasilewski Z, Fafard S and McCaffery J 1999 *J. Cryst. Growth* **201/202** 1131–5
[31] Solomon G, Komarov S, Harris J Jr and Yamamoto Y 1997 *J. Cryst. Growth* **175/176** 707–12
[32] Cockayne D, Liao X and Zou J 2001 *Inst. Phys. Conf. Ser.* **169** 77–83
[33] Egerton R F 1986 *Electron Energy-Loss Spectroscopy in the Electron Microscope* (New York: Plenum) chapter 5 (ISBN 0-306-42158-5)
[34] Gass M H, Papworth A J, Bullough T J and Chalker P R 2004 *Ultramicroscopy* submitted
[35] Johnson D W 1975 *J. Phys. A: Math. Gen.* **8** 490
[36] Gass M, Papworth A J, Joyce T B, Bullough T J and Chalker P R 2004 *Appl. Phys. Lett.* **84** 1453
[37] Vurgaftman I, Meyer J R and Ram-Mohan L R 2001 *J. Appl. Phys.* **89** 5815
[38] Pan Z, Li L H, Lin Y W, Sun B Q, Jiang D S and Ge W K 2001 *Appl. Phys. Lett.* **78** 2217
[39] Hetterich M, Dawson M D, Egorov A Yu, Bernklau D and Riechert H 2000 *Appl. Phys. Lett.* **76** 1030
[40] Hai P N, Chen W M, Buyanova I A, Xin H P and Tu C W 2000 *Appl. Phys. Lett.* **77** 1843
[41] Zhang Y, Mascarenhas A, Xin H P and Tu C W 2000 *Phys. Rev.* B **61** 7479
[42] Mazzucato S *et al* 2003 *J. Appl. Phys.* **93** 2440
[43] Skierbiszewski C *et al* 2000 *Appl. Phys. Lett.* **76** 2409
[44] Lindsay A and O'Reilly E P 1999 *Solid State Commun.* **122** 443
[45] Young D L, Geisz J F and Coutts T J 2003 *Appl. Phys. Lett.* **82** 1236